Quantum critical points in ferroelectric relaxors: Stuffed tungsten bronze $K_3Li_2Ta_5O_{15}$ and lead pyrochlore ($Pb_2Nb_2O_7$)

Rebecca M. Smith,[1] Jonathan Gardner,[1] Finlay D. Morrison,[1] S. E. Rowley,[2,3] Catarina Ferraz,[4] M. A. Carpenter,[5] Jiasheng Chen,[2] Jack Hodkinson,[2] Siân E. Dutton,[2] and J. F. Scott[1,6]

[1]*School of Chemistry, University of St. Andrews, St. Andrews, KY16 9ST, United Kingdom*
[2]*Cavendish Laboratory, University of Cambridge, J. J. Thomson Avenue, Cambridge, CB3 0HE, United Kingdom*
[3]*Centro Brasileiro de Pesquisas Físicas, Rua Dr Xavier Sigaud 150, Rio de Janeiro, 22290-180, Brazil*
[4]*UFRJ, Estr. de Xerém 27, Xerém, Duque de Caxias, Rio de Janeiro, 25245-390, Brazil*
[5]*Department of Earth Sciences, University of Cambridge, Downing Street, Cambridge, CB2 3EQ, United Kingdom*
[6]*School of Physics, University of St. Andrews, St. Andrews, KY16 9SS, United Kingdom*

We have synthesized ceramic specimens of the tetragonal tungsten bronze $K_3Li_2Ta_5O_{15}$ (KLT) and characterized its phase transition via x-ray diffraction, dielectric permittivity, resonant ultrasonic spectroscopy, and heat capacity measurements. The space group of KLT is reported as both $P4/mbm$ and $Cmmm$ with the orthorhombic distortion occurring when there are higher partial pressures of volatile K and Li used inside the closed crucibles for the solid state synthesis. The data show strong relaxor behavior, with the temperature at which the two dielectric relative permittivity peaks decreasing, with $104 \geqslant T_{m1} \geqslant 69\,\mathrm{K}$ and $69 \geqslant T_{m2} \geqslant 46\,\mathrm{K}$ as probe frequency f is reduced from 1 MHz to 316 Hz. F tests show that the data satisfies a Vogel-Fulcher model better than Arrhenius with an extrapolated freezing temperature for ε' and ε'' of $T_{f1} = +15.8$ and $-11.8\,\mathrm{K}$ and $T_{f2} = -5.0$ and $-15.0\,\mathrm{K}$ for $f \to 0$ (tending to dc). This difference between T_f from real and imaginary values, albeit counterintuitive, is mandatory, according to the theory of Tagantsev. Therefore, by tuning frequency, the transition could be shifted to absolute zero, suggesting KLT has a relaxor-type quantum critical point. In addition, we have reanalyzed the conflicting literature for $Pb_2Nb_2O_7$ pyrochlore which suggests that this also has a relaxor-type quantum critical point since the freezing temperature from the Vogel-Fulcher fitting is below absolute zero. Since the transition temperature evidenced in the dielectric data at approximately 100 kHz shifts below 0 K for very low frequencies, this transition would not be seen with heat capacity data collected in the zero-frequency (dc) limit. Both of these materials show promise for possible new relaxor-type quantum critical points with nonperovskite based structures.

I. THE SEARCH FOR NEW QUANTUM CRITICAL POINT (QCP) FERROELECTRICS INCLUDING RELAXOR QCPS

Quantum critical point (QCP) studies of ferroelectrics have been limited to a few crystal structures, emphasizing perovskite oxides. The drive to find new QCPs with ferroelectrics (FEs) are of interest due to the likelihood that they will exhibit novel electrical and thermal properties over wide ranges in temperature and tuning parameters, similar to what is seen in more widely studied magnetic counterparts. However, as the dynamical exponent is 1 for displacive FE rather than 3 for itinerant ferromagnets, the understanding and modeling of their properties are likely to be more complex, since real systems can exceed the upper and lower critical dimensionality [1]. For a QCP to occur, the transition should be driven by quantum fluctuations rather than classical fluctuations, and such quantum fluctuations tend to dominate in a region just above 0 K. Interest in ferroelectric quantum critical points has grown rapidly in the past several years, with emphasis upon perovskites [1,2] and several other materials, including hexaferrites [3–6] and organic or molecular crystals [7–10]. However, the QCPs studied thus far do not include many crystal families, and with one recent exception [11], no glassy relaxors. The advantage of relaxor QCPs is that their

dielectric permittivity peaks at a temperature that is strongly dependent upon probe frequency (Hz to MHz), and hence the permittivity divergence can be driven exactly through $T = 0\,\mathrm{K}$ via frequency, permitting an extra dimension of experimental phase space to be probed. QCP systems with glassy, highly degenerate ground states at $T = 0\,\mathrm{K}$ are of special interest. Our collaborators have previously shown that one can drive the apparent phase transition temperature in relaxors through $T = 0$ by changing applied frequency [3,12].

For relaxor ferroelectrics, the Vogel-Fulcher equation [13–15] is used to model the dielectric data. Although this was originally an empirical model extending Arrhenius-type relaxations, it has been retroactively derived theoretically from different assumptions. Two recent and different post facto derivations are given in [16,17]. In the literature such Vogel-Fulcher fits to relaxor data (such as PMN) generally give finite freezing temperatures T_f. In the present context, the main point of Vogel-Fulcher modeling to quantum critical point systems is that they give freezing temperatures below absolute zero; this is not unphysical but merely implies that the ground state at $T = 0\,\mathrm{K}$ lacks long range order, as expected for QCP.

In the present work we extend such studies to tetragonal tungsten bronze-type structures (TTBs), a broad family of device materials and pyrochlores. In a search for new FE QCP,

it is preferable to start with FEs with known transitions near 0 K. KLT and $Pb_2Nb_2O_7$ pyrochlore may have QCP transitions with T_c reported as 7 and 15 K respectively; however, to confirm the behavior driving the transition, permittivity versus temperature data are required [5,11,18].

II. TETRAGONAL TUNGSTEN BRONZE-TYPE STRUCTURES INCLUDING POTASSIUM LITHIUM TANTALATE

Tetragonal tungsten bronzes (TTBs) have a structure related to perovskites (ABO_3) created by rotation of some of the columns of octahedra, which maintains a corner sharing network of BO_6 octahedra but generates pentagonal A2, square A1, and trigonal C channels along the c axis (most often the polar axis), giving an overall formula of $A2_2A1C_2B_5O_{15}$ [19]. Tetragonal in TTBs refers to the highest symmetry structure likely to be observed with the crystal structure which happens in their highest temperature phase not necessarily their room temperature phase. A sites are occupied by medium to large cations such as Ba, Ca, K, or Na ions, with larger cations preferentially occupying the larger A2 site. The triangular channels are very small, and therefore normally empty, but can contain Li [20]. Several niobate- and tantalate-based TTBs are of interest, with B ions being Nb or Ta, as they have been reported as ferroelectrics (FEs), both normal and relaxor type. Unfilled TTBs with composition of $[Ba_{1-x}(Sr/Pb)_x]_5Nb_{10}O_{30}$ are reported [21,22] as having relaxor behavior for $x < 0.5$ for Sr/Ba versions with $T_m = 333$ K at 1 MHz and $x = 0.25$. Samples with $x > 0.5$ and Pb/Ba analogs are normal ferroelectrics (FEs) with $T_c = 333-823$ K. All of the Sr/Ba and Ba/Pb versions have incommensurate structures, whether or not relaxor behavior is seen. The BO_6 octahedra tilts generate the incommensurate superstructures rather than variations in filling sequence, with the Ba, Sr, or Pb ions and partial occupancies in A sites. Similarly, empty $Ba_4RE_{0.67}Nb_{10}O_{30}$ (RE = La, Nd, Sm Gd, Dy, and Y) TTBs [21] have vacancies reported in some of the A1 and all the C sites. For La, relaxor behavior is seen with the dielectric maximum at temperature $T_m = 297$ K at 1 MHz, whereas other RE compounds are reported as normal FEs with T_c ranging from 406 to 537 K—a size effect due to decreasing size of RE ions as atomic number increases. The filled $Ba_4Na_2Nb_{10}O_{30}$ TTB has all A2 and A1 sites occupied by Ba and Na, respectively, with only the C sites vacant. In $Ba_4Na_2Nb_{10}O_{30}$ there are a large number of phase transitions, starting at high temperatures with a tetragonal paraelectric phase and finishing at cryogenic temperatures (<10 K) with a (larger-cell) tetragonal phase. The four or five phases at intermediate temperatures include commensurate and incommensurate (both $1q$ and $2q$ modulation) phases and are mostly orthorhombic. These distortions are, however, all with the xy plane normal to the spontaneous polarization with $1q$ modulation being incommensurate in either x or y direction with $2q$ incommensurate with identical modulation in both x and y directions. So all the phases below the uppermost are ferroelectric (with polarization P along the z axis). (Note that after a series of orthorhombic phases at intermediate temperatures, $Ba_2NaNb_5O_{15}$ reverts to a tetragonal $P4nc$ commensurate ground state at lowest temperatures [23]; this

"reverse symmetry" orthorhombic-tetragonal cooling transition involves a unit-cell doubling.)

$K_3Li_2Nb_5O_{15}$ (KLN) is a possible "stuffed" TTB since the stoichiometric material has K on all the A2 and A1 sites and Li on all the C sites; however, several authors [24–28] suggest that an excess of Nb is required to form single-phase samples. Therefore the structure either has vacancies and/or mixing of the crystallographic site occupancy. The higher temperature transition around 750 K for KLN is from $4/mmm$ to $4mm$, and the low-temperature transition at 80 K, is from $4mm$ to m. However, in contrast to other previously mentioned TTBs, except Pb-containing ones, the lower structural distortion is along the polar axis, not orthogonal to it [29]. The difference at low temperatures from other tungsten bronzes may arise from its decreased flexibility in the xy plane due to the stuffed C channels with Li; therefore the same situation may occur for other stuffed TTBs. However, this explanation is not generally true since low-temperature $4mm$ to m is also reported for TTBs without filled C channels but with other complicating ions such as Pb or Bi [30–32] with stereochemical lone pairs.

$K_3Li_2Ta_5O_{15}$ (KLT), an analog of KLN, is reported to form as a single-phase sample without excess Ta due to the decrease in electronegativity of Ta compared to Nb [24], not due to a size difference, as both ionic radii of Nb and Ta are 0.64 Å [33]. KLT has been studied as a single crystal [34] and dense ceramic [24] samples with the structures shown in Fig. 1; but its structure remains contentious as both $Cmmm$ and $P4bm$ were reported. However, later authors could not determine orthorhombic distortion with their PXRD data. The single crystal's electrical properties showed $T_c = 7$ K, with a polarization-electric field hysteresis loop occurring below T_c at 50 Hz. Whether there is a frequency dependence in dielectric permittivity is unknown since published papers
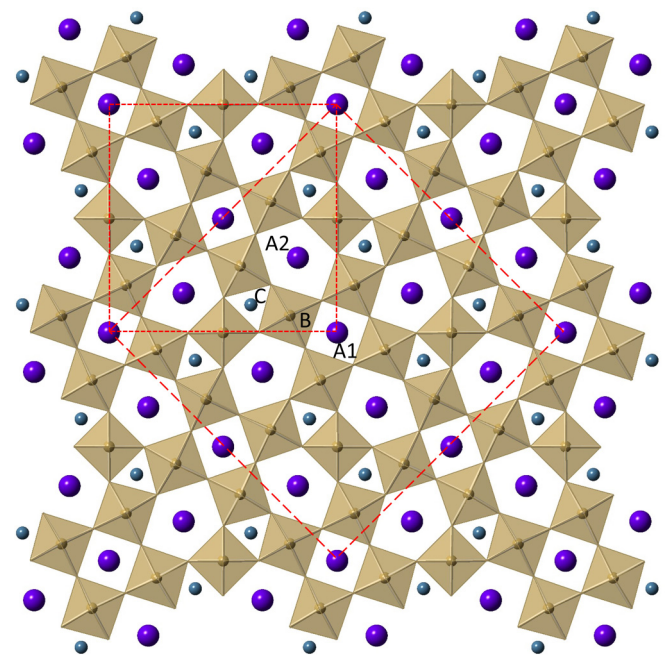

FIG. 1. Theoretical [24,34] TTB structures of KLT for *ab* plane in $P4/mbm$ (short dashes) and $Cmmm$ (long dashes) space groups. Cell parameters for $P4/mbm$ as $a = 12.60$ Å, $c = 3.936$ Å and $Cmmm$ as $a = 17.78$ Å, $b = 17.83$ Å, $c = 3.931$ Å.

studied only one frequency. The substitution of Nb for Ta in any of these TTBs has a drastic effect upon its Curie temperature, for example increasing it from $T_c = 7$ K in KLT to $T_c = \sim 753$ K in KLN [35–40]. This extremely large shift in Curie temperature for Nb/Ta substitution has not yet been modeled or explained by DFT calculations; note that there is no change in ionic radius, so the large change in T_c is presumably a mass or electronegativity effect.

Fukuda reports [34] that Ta-rich members of the $K_3Li_2(Ta_xNb_{1-x})_5O_{15}$ solid solution undergo a tetragonal to orthorhombic transition with falling temperatures from 523 K for higher values of x to 295 K for $x = 0.55$, with the generation of cross-hatch twins above $x = 0.7$. The symmetry change is most probably $P4/mbm$-$Cmmm$. It is inevitable that ferroelastic twin walls parallel to (110) and (1 −1 0) of the parent tetragonal structure will be present in orthorhombic KLT crystals which were synthesized at high temperatures and then cooled through the transition point.

A. Experimental methods

1. Synthesis, PXRD, and SEM/EDX

KLT was synthesized using stoichiometric amounts of dried K_2CO_3 (Sigma Aldrich 99%), Li_2CO_3 (Alfa Aesar 99%), and Ta_2O_5 (Alfa Aesar 99%). The powder was ball milled for 2 h in a planetary ball mill at 600 rpm in ethanol, and then pressed into loose 1 g pellets to be reacted inside 4 ml closed crucibles surrounded by sacrificial powder (composition below) at 1073 K (ramp rate of $10\,K\,min^{-1}$) for 2 h. Pellets were ground in an agate mortar and pestle before being pressed into 0.4 g pellets in a uniaxial press at 500 psi before sintering at 1573 K for 4 h. K and Li are volatile, so they escape from the powder or pellets during high temperature sintering. Therefore, attempts were carried out with 17% excess or deficient K and Li for the surrounding sacrificial powders compared to stoichiometric KLT, creating higher or lower K and Li partial pressures, respectively, inside the crucibles. Other than the room temperature PXRD patterns and SEM/EDX analysis, all data are reported on samples made with 17% excess K and Li in the sacrificial powder.

Room temperature PXRD data from pellet surfaces were taken on a PANalytical Empyrean diffractometer in the range $2\theta = 5°$−$90°$ with Cu $K_{\alpha 1}$ source and step size $\Delta 2\theta = 0.017°$. Variable temperature measurements $T = 12$−300 K were completed on crushed powder in a Bruker D8 Advance diffractometer, using an Oxford Cryosystems PheniX stage from $2\theta = 10°$−$110°$ with step size of $\Delta 2\theta = 0.0102°$ and Cu K_α sources, $\lambda = 1.54\,Å$. Rietveld refinements [41] were performed using GSAS/EXPGUI [42,43]. Peak shapes were modeled using a pseudo-Voigt function, and the background fit using a 12th order Chebyschev polynomial. To account for changes in intensity due to preferred orientation along [00l], a spherical harmonic order 28 model was used.

Scanning electron microscopy (SEM) and energy-dispersive x-ray spectroscopy (EDX) were undertaken on the same polished sample surface as the room temperature PXRD. This analysis used a Jeol JSM 5600 scanning electron microscope with an accelerating voltage of 30 kV and an Oxford Inca EDX system. For EDX analysis, three separate areas of the pellet were used and in each area seven different spectra

were collected, giving 21 spectra in total. Each spectrum was analyzed twice, with and without the O peak being used in the calculations. The values for O, as expected, seemed to be unrealistic so are not reported. As results were around the stoichiometric KLT ratios, PXRD GSAS/EXPGUI refinements were undertaken without altering K occupancies.

2. Specific heat data

The specific heat measurements were undertaken on two sets of equipment, one of which was a Quantum Design PPMS system using the standard relaxation technique on a pellet sample with a mass of 0.2729 g; the other used 0.0031 g of crushed powder from a pellet. This is sufficiently large that the measurements should be dominated by its intrinsic response.

3. Dielectric properties and immittance spectroscopy

The circular faces of pellets for electrical measurements were polished with silicon carbide abrasive paper before applying silver electrode paste (RS components) and curing for $\geqslant 15$ min at 423 K for permittivity measurements. Relative permittivity and dielectric loss measurements were performed using an HP 4192A impedance analyzer over frequency range from 100 Hz to 1 MHz, from 15 to 300 K with the sample mounted in a Janis cryostat with a closed-cycle helium refrigerator. The dielectric peak maxima were extracted from a ninth order polynomial around each peak and solved iteratively using the Vogel-Fulcher relationship for both relative (real) permittivity and dielectric loss (imaginary component of complex permittivity).

For immittance measurements, gold electrodes were sputtered onto the faces which are able to withstand higher temperatures. Immittance measurements using a Wayne Kerr 6500B impedance analyzer were undertaken from 303 to 832 K approximately every 5 K in the frequency range of 25 Hz to 1.28 MHz using a custom-made sample holder inside a Carbolite furnace. The data were extracted using ZView software to generate an Arrhenius plot and, from linear fits, activation energies determined for each range.

4. Resonant ultrasound spectroscopy

The sample used for resonant ultrasound spectroscopy (RUS) measurements was in the form of a colorless rectangular parallelepiped with dimensions $2.756 \times 2.757 \times 1.046\,mm^3$ and mass 0.0345 g, which had been cut from a larger ceramic fragment. Rounding of some edges was clearly due to falling away of individual crystals, indicating a slight propensity for disaggregation.

The RUS technique has been described in detail by Migliori and Sarrao [44] and the instrument used in the present study by Schiemer *et al.* [45] and Evans *et al.* [46]. Low temperatures are delivered by a cryogen free Oxford Instruments Teslatron cryostat, and the RUS head sits in a sample chamber containing a few millibars pressure of helium gas to provide thermal exchange with the sample. The KLT parallelepiped was placed in the RUS head with piezoelectric transducers in light contact with the pair of its largest faces. Primary data were collected in the frequency range 10–1200 kHz with 65 000 data points per spectrum. An automated sequence of cooling and heating, with a settle time of 60 s for thermal equilibration before data

collection at each set point, was as follows: cooling from 295 to 5 K in 5 K steps, followed by heating from 4 to 30 K in 2 K steps, 31 to 65 K in 1 K steps, 70 to 295 K in 5 K steps.

Analysis of the primary spectra was conducted offline using the software package Igor (Wavemetrics) to fit individual resonance peaks with an asymmetric Lorentzian function. The square of the peak frequency f of each peak scales with the elastic constant which determine the distortions involved. The peak width at half maximum height Δf provides a measure of acoustic loss as the inverse mechanical quality factor Q^{-1} which is taken here to be $\Delta f / f$. The normal modes of the sample are governed predominantly by shearing, typically with only small contributions from breathing motions, and variations of f^2 for a polycrystalline sample are therefore dependent predominantly on the shear modulus, with only small contributions from the bulk modulus

B. Results

1. PXRD and SEM/EDX

The partial pressures of volatile K and Li affect whether an orthorhombic distortion occurs from $P4/mbm$ to $Cmmm$ in the room temperature PXRD patterns. SEM/EDX was undertaken on both of these surfaces to determine the ratios for K:Ta with ideal values being 3:5. However, obtained ratios varied depending on whether the observed O peak was removed from calculations.

At lower K and Li partial pressures, the crystal structure refines in $P4/mbm$ [$wR_p = 0.1132$, $R_p = 0.0786$, $\chi^2 = 4.642$, $R(F^2) = 0.0535$] with no obvious splitting in peaks seen [Fig. 2(a)]. Attempts at refining in orthorhombic $Cmmm$ space group resulted in no major improvements, confirming that tetragonal $P4/mbm$ is the correct space group based on the current PXRD data. The SEM/EDS ratios are 2.51:5 or 3.01:5 (range 2.31–2.81:5 or 2.83–3.33:5) with and without O peak used to calculate atomic percentages, respectively.

When higher K and Li partial pressures are used, clear peak-splitting occurs in the PXRD pattern [Fig. 2(b)] and an orthorhombic space group of $Cmmm$ [$wR_p = 0.0976$, $R_p = 0.0619$, $\chi^2 = 3.012$, $R(F^2) = 0.0470$] is obtained, giving an orthorhombic distortion of 0.21%. The SEM/EDS ratios with and without O peak are 2.60:5 or 3.14:5 (range 2.30–2.89:5 or 2.85–3.41:5), showing a higher K content.

All further results are reported on samples made under higher partial pressures of K and Li because that gave lower PXRD GSAS/EXPGUI refinement parameters and more ideal averaged ratios according to SEM/EDX were obtained. Variable temperature PXRD was undertaken from room temperature down to 12 K, which showed no obvious changes in cell parameters apart from an increase in orthorhombic distortion with decreasing temperature [Fig. 2(c)]. We remind readers that phase transitions in solids need not change crystal symmetry at all; there are many solid state phase transitions (slightly first order) which are isosymmetric, including one in $BiFeO_3$. Phase transitions are defined thermodynamically, not crystallographically.

2. Specific heat capacity

The heat capacity data are shown in Fig. 3. The temperature dependence of the heat capacity scales as T^3 at low tempera-
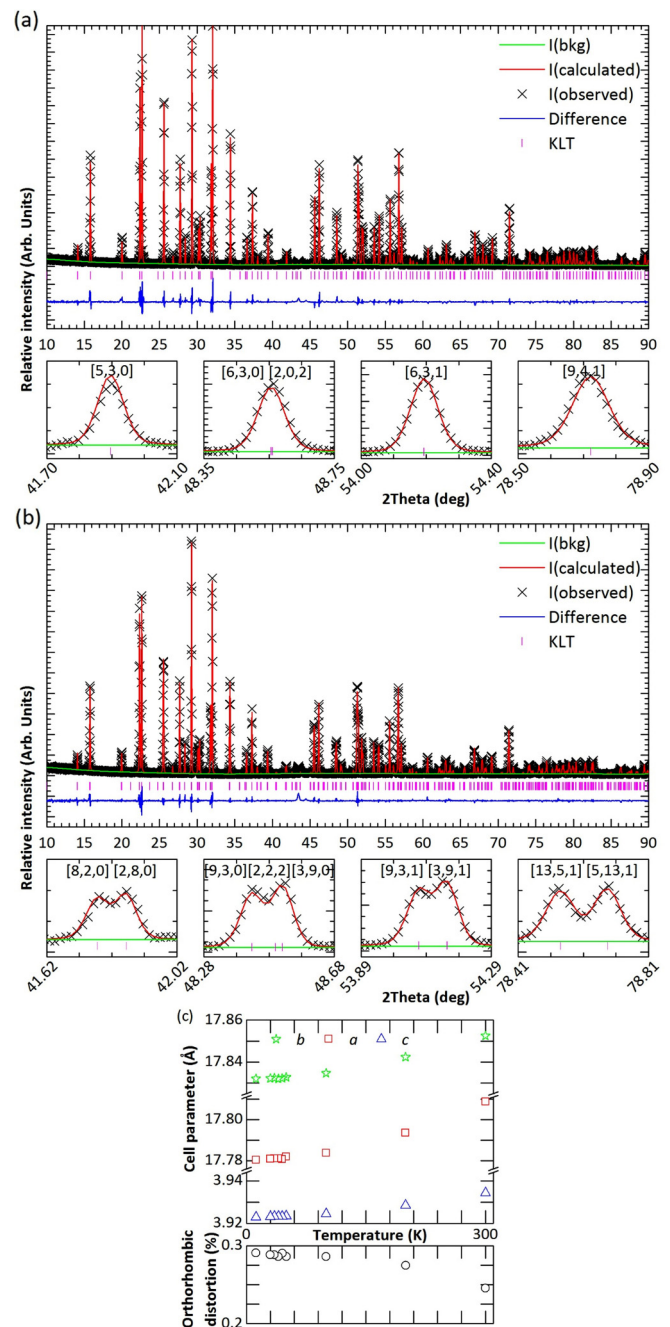

FIG. 2. Room temperature PXRD from the surface of pellets sintered under (a) lower and (b) higher partial pressures of K and Li in space group $Cmmm$ and (c) variable temperature PXRD of powder made by grinding up higher partial pressure K and Li pellet refined in $Cmmm$ space group.

tures before reaching a lower power at higher temperatures. No anomalies were observed over the temperature range measured, consistent with the absence of a phase transition in the low frequency (dc) limit.

3. Dielectric data

The dielectric data [Fig. 4(a)] showed two frequency dependent peaks in both the relative (real) permittivity ε' and loss
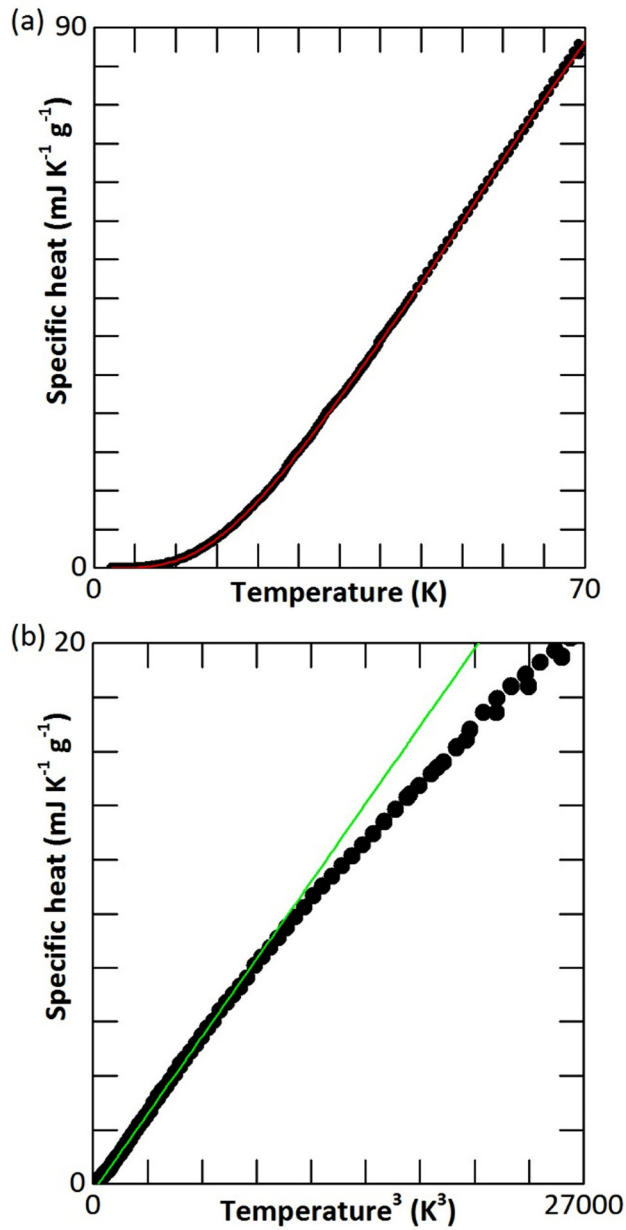
FIG. 3. (a) The heat capacity plotted versus temperature. No anomaly is observed over the full temperature range measured, consistent with a ferroelectric relaxor freezing temperature suppressed below 0 K. As shown in (b) a T^3 dependence is observed at low temperatures, as expected from the contribution of acoustic phonons.

(imaginary permittivity) ε'' at temperatures of $T_{m1} = 59.9$ K and $T_{m2} = 90.9$ K in ε' at 100 kHz; both peaks exhibit relaxor behavior. In an aim to characterize this relaxor behavior several types of fits were undertaken (Table I) to model the relaxor-type peak maxima in both the relative and imaginary permittivity data. Vogel-Fulcher fits [Fig. 4(b)] with variable freezing temperatures significantly reduce the error between the experimental maxima and the fitted values (SSR or sum of squared residuals) when compare to Arrhenius fits (where the freezing temperature is fixed to absolute zero). An f test to the data [47], with 95% confidence interval, confirmed that the

FIG. 4. (a) Relative (real) permittivity ε' and imaginary permittivity ε'' on heating, with arrow showing increasing frequency (316 Hz–1 MHz using six frequencies per decade). (b) Vogel-Fulcher fits to both relative and imaginary permittivity peaks, giving values reported in Table I. (c) Curie-Weiss behavior plot above the higher temperature dielectric peak, with linear fitting to obtain a Curie constant of 70 300−74 100 K depending on frequency fitted to range above T_{m2} (present work.)

TABLE I. Vogel-Fulcher (VF), Arrhenius (Arr.), and critical power-law (crit.) fits to relative permittivity ε' from 316 Hz to 1 MHz and Vogel-Fulcher and Arrhenius fits for imaginary been permittivity from 1 or 1.47 kHz (T_{m2} or T_{m1}) to 1 MHz due to limitations of equipment. The errors in calculated values were derived from standard deviation errors in the value of T_m used. SSR for critical power law was minimized as Hz^2 before $\ln{(Hz)}^2$ values were calculated.

Fit type	Parameter (units)	ε' T_{m1}	ε'' T_{m1}	ε' T_{m2}	ε'' T_{m2}
VF $f = f_0 e^{-\frac{E_a}{k(T_m - T_f)}}$	$f_0 (Hz)$	4.54×10^{10}	2.26×10^{10}	2.81×10^{13}	3.97×10^{13}
	$E_a (eV)$	0.05(1)	0.08(1)	0.16(1)	0.17(1)
	$T_f (K)$	+15.8(11)	−11.8(5)	−5.0(3)	−15.0(7)
	SSR [$\ln{(Hz)}^2$]	0.0267(19)	0.0041(2)	0.0062(4)	0.0060(3)
Arr. $f = f_0 e^{-\frac{E_a}{kT_m}}$	$f_0 (Hz)$	1.41×10^{13}	4.82×10^{10}	8.53×10^{12}	1.46×10^{13}
	$E_a (eV)$	0.10(1)	0.05(1)	0.14(1)	0.12(1)
	SSR [$\ln{(Hz)}^2$]	0.2485(135)	0.0653(30)	0.0121(7)	0.0098(5)
Crit. $f = a(T_m - T_0)^b$	$T_0 (K)$	42.02(228)		60.04(326)	
	A	$1.06 \times 10^{-2}(6)$		$2.07 \times 10^{-4}(11)$	
	b	5.56(30)		5.89(32)	
	SSR (Hz^2)	$1.18 \times 10^8(6)$		$6.45 \times 10^9(35)$	
	SSR [$\ln{(Hz)}^2$]	13.88(539)		4.21(164)	

Vogel-Fulcher fits are mathematically superior to Arrhenius fits (nearest being 106% of tabled values); this test incorporates the different number of adjustable parameters in the two models. A critical power-law fit is an alternative, which for ε' does not give as low an error (SSR) or as good a fit by eye as either of the other two types of fit. When extracting the peak maxima, it became obvious that the relative permittivity peaks overlap more than imaginary ones, so both were extracted and analyzed. The attempt frequencies f_0 are quite uncertain. By extrapolation of Vogel-Fulcher fits, the vertical asymptote is the freezing temperature T_f where an extrapolated glassy structural transition may occur. The horizontal asymptote is the fundamental attempt frequency and T_{m2} has a higher value than T_{m1}. This difference in T_{m1} and T_{m2} is counterintuitive (how can there be two different freezing temperatures?), but it is absolutely mandatory for relaxors, as explained by Tagantsev in 1994 [48]. Moreover, Tagantsev shows that T_f found from the imaginary part of the dielectric function must always be lower than that from the real part, as we find here and in our earlier work on hexaferrites. The reasons for this are subtle, but we remind readers that there are many subtleties at liquid-solid transitions, such as the Kauzmann paradox.

The frequency f_0 in Vogel-Fulcher fits is not often reliable, because the least-squares fitting is not very sensitive to this number. However, to be physically plausible it should be on the order of a phonon frequency. Optical phonons of long wavelength are typically 10^{13} Hz ($300 \, cm^{-1}$), and acoustic phonons of order 10^{11} Hz ($3 \, cm^{-1}$), as observed here. The data above the higher temperature dielectric peak fit Curie-Weiss behavior [Fig. 4(c)] which, for the above values of T_{m2}, gives a Curie constant of $7.1–7.4 \times 10^4$ K, depending on frequency, which is reasonable for an oxide ferroelectric [49] (about 70% of that in $BaTiO_3$ [50]).

4. Immittance spectroscopy

Immittance spectroscopy generated semicircles and peaks in the measurement range above 575 K [Figs. 5(a)–5(f)]. From the Arrhenius plot [Fig. 5(g)] the activation energies were determined for the two different ranges of 575–671 K and 723–840 K as there is a change in gradient between these ranges. Values of the activation energies for the range 575–671 K are 0.90, 0.90, 0.89, and 0.89 eV for M'', Z'', M^*, and Z^* formalisms, respectively. Activation energies for the higher temperature range are 0.77, 0.76, 0.78, and 0.76 eV, similar for M'', Z'', M^*, and Z^* formalisms. These numbers are typical of oxide ferroelectrics and often arise from oxygen vacancies; but as discussed below, they are also typical of Li-ion conduction.

5. RUS

Segments of the primary RUS spectra are shown as a stack in Fig. 6. Each spectrum has been offset up the y axis in proportion to the temperature at which it was collected during cooling, and blue curves are fits of the asymmetric Lorentzian function used to determine values of f and Δf. There is a tendency for all the resonances to appear in pairs because of a near degeneracy arising from the close similarity in two of the edge dimensions of the sample. All the resonances follow essentially the same trend of significant elastic softening with falling temperature to a clear minimum at ∼50 K, followed by recovery.

Figure 7(a) shows variations of f^2 and Q^{-1} throughout the complete sequence of cooling and heating for resonances with frequencies near 65, 550, and 600 kHz. There are four distinctive features. First, there is an initial trend of reducing f^2, corresponding to softening of the shear modulus, as temperature is lowered, with a maximum softening of ∼30%. This ends with an abrupt change to a trend of stiffening by up to ∼15% below ∼50 K. Slightly regular variations in f^2 through ∼50 K are accompanied by a peak in Q^{-1} which returns to baseline values below ∼25 K and above ∼65 K. Second, there is difference of ∼5 K between heating and cooling for the temperature at which the maximum in Q^{-1} occurs (∼40 K cooling, 47 K heating in the case of the peak near 65 kHz) and for the temperature at which the main break in slope of f^2 occurs (45 K cooling, 52 K heating, ∼65 kHz). Third, there both f^2 and Q^{-1} display a distinct hysteresis in the
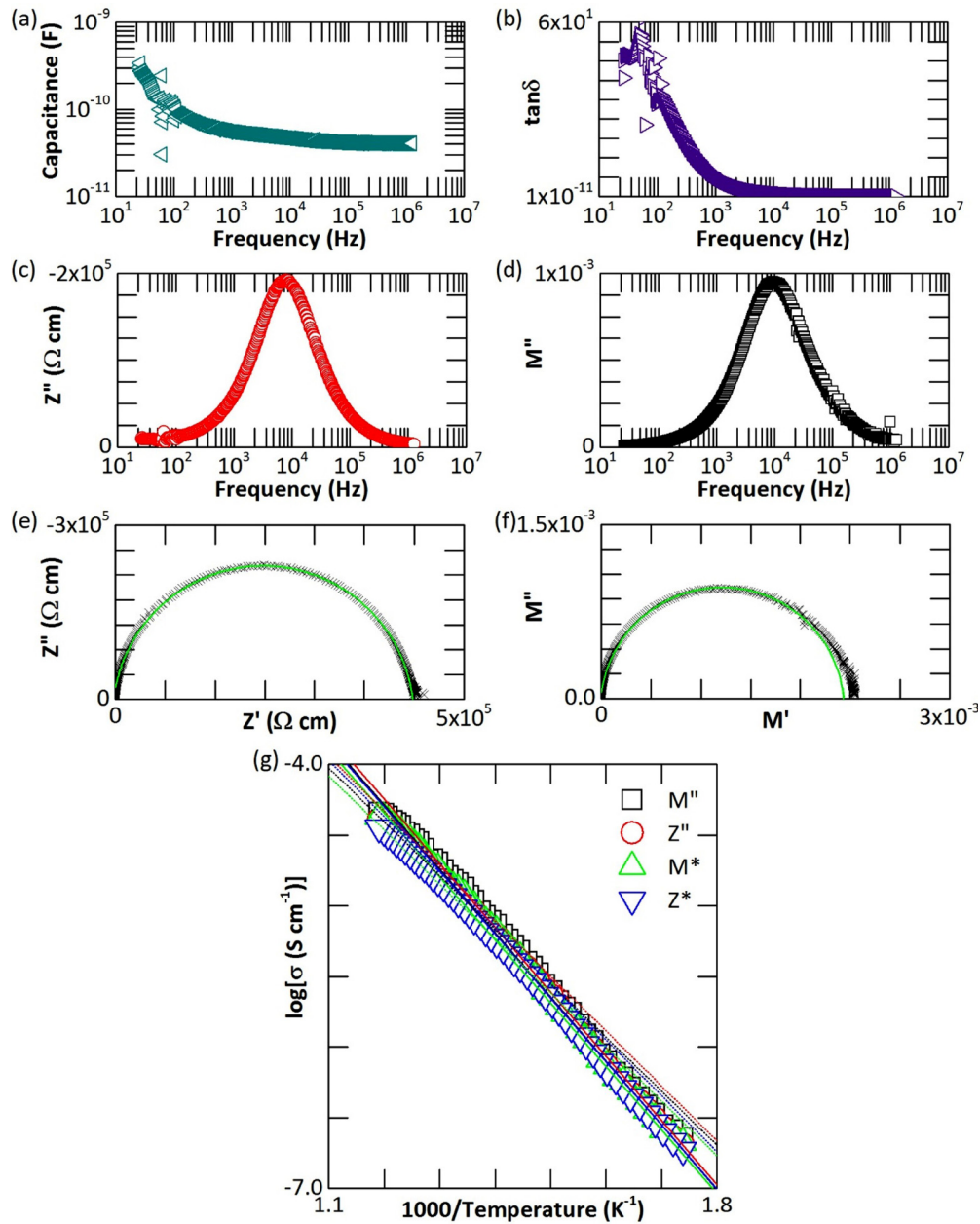
FIG. 5. Imittance spectroscopy plots: (a)–(f) example of Nuquist and Bode plots at 671 K, with single semicircles corresponding to domain permittivity and a relaxation time of $t \approx 18\,\mu s$; $R \approx 0.4\,\text{M}\Omega$; $C \approx 47\,\text{pF}$. We interpret this as a response in a grain and no evidence of grain boundary relaxation. The data are extracted to generate an Arrhenius plot (g) from which activation energies can be determined.

temperature interval between $\sim 50\,\text{K}$ and room temperature. The elastic stiffness is lower and the loss higher during heating than during cooling. Finally, there is a gradual increase in the baseline values of Q^{-1} with increasing temperature and there is a broad peak near 250 K during cooling and near 280 K during heating.

Details of the changes in f^2 and Q^{-1} are shown for the resonance peak near 65 kHz in Fig. 7(b). The irregular pattern of variations in the interval ~ 25–$65\,\text{K}$ appears to show a sequence of steplike changes in f^2 accompanied by a series of overlapping peaks in Q^{-1}, which would correspond to a sequence of, perhaps, three Debye freezing events. These can be represented, for the variation of temperature at approximately

constant frequency, by [51–54]

$$Q^{-1}(T) = Q_{max}^{-1} \left[\cosh \left\{ \frac{E_a}{\text{R}r_2(\beta)} \left(\frac{1}{T} - \frac{1}{T_{max}} \right) \right\} \right]^{-1} .$$

Q_{max}^{-1} is the maximum value of Q^{-1}, occurring at T_{max}, E_a is an activation energy, and $r_2(\beta)$ is a width parameter to describe a spread of relaxation times (as set out in Table 4-2 of Nowick and Berry [55]). The value of $r_2(\beta)$ is 1 for a single relaxation time but increases as the range of relaxation times broadens. A single smooth curve shown in gray in Fig. 7(b) has $Q_{max}^{-1} = 0.0145$, $T_{max} = 47.5\,\text{K}$, and $E_a/r_2(\beta) = 0.1\,\text{eV}$.
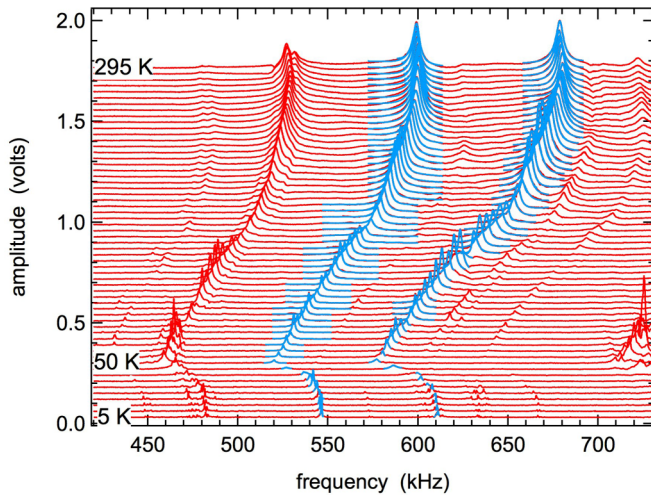
FIG. 6. Stack of primary spectra collected at 5 K intervals during a cooling sequence. The left axis is the amplified signal from the detecting transducer and the bottom axis is the frequency of the ac signal applied to the driving transducer. Each spectrum has been offset up the y axis in proportion to the temperature at which it was collected. Blue curves are fits of the asymmetric Lorentzian function used to determine values of f and Δf.

The overall peak in Q^{-1} could be represented by three or four overlapping peaks with about the same activation energy or by a single loss process with $E_a/r_2(\beta) = 0.027$ eV. If E_a is taken to be 0.1 eV, by comparison with results from dielectric spectroscopy, $r_2(\beta) = 3.71$ is obtained. The correlation of steplike increases at $\sim$35, 42, and 48 K in f^2 with the location of possible overlapping peaks in Q^{-1} suggests that the correct description would be of a sequence of Debye-like freezing processes.

C. Discussion

In the existing prior literature, both space groups $P4/mbm$ and $Cmmm$ are reported [24,34] for ceramic and single crystal KLT samples using XRD analysis at room temperature. The PXRD room temperature results reported here suggest that both space groups can exist depending on the reaction conditions used with KLT synthesized with higher partial pressures of volatile K and Li lead to an orthorhombic distortion. Using SEM/EDX, it is possible to determine the K:Ta ratios with and without accounting for the visible O peak, but not Li, in pellets made under these conditions. This shows that the higher partial pressures results in higher amounts of K on the polished pellet's surface when compared to pellets sintered with lower partial pressures. This implies that the orthorhombic distortion may be linked to K content in the structure. Orthorhombic distortions can occur when the A1 site distorts from the perfect square channel, and in this case K on the A1 site would explain the existence of orthorhombic distortions for higher K content. In TTBs it is not unprecedented to have orthorhombic distortion and expansions of the unit cells from the $P4/mbm$ ($Z = 2$) cell. Other examples [56–62] include $Ba_2NaNb_5O_{15}$ or $Ba_4La_{0.67}Nb_{10}O_{30}$; $Ba_2NaNb_5O_{15}$ has five structural phase transitions as the temperature is lowered, some incommensurate, all of which are orthorhombic distortions
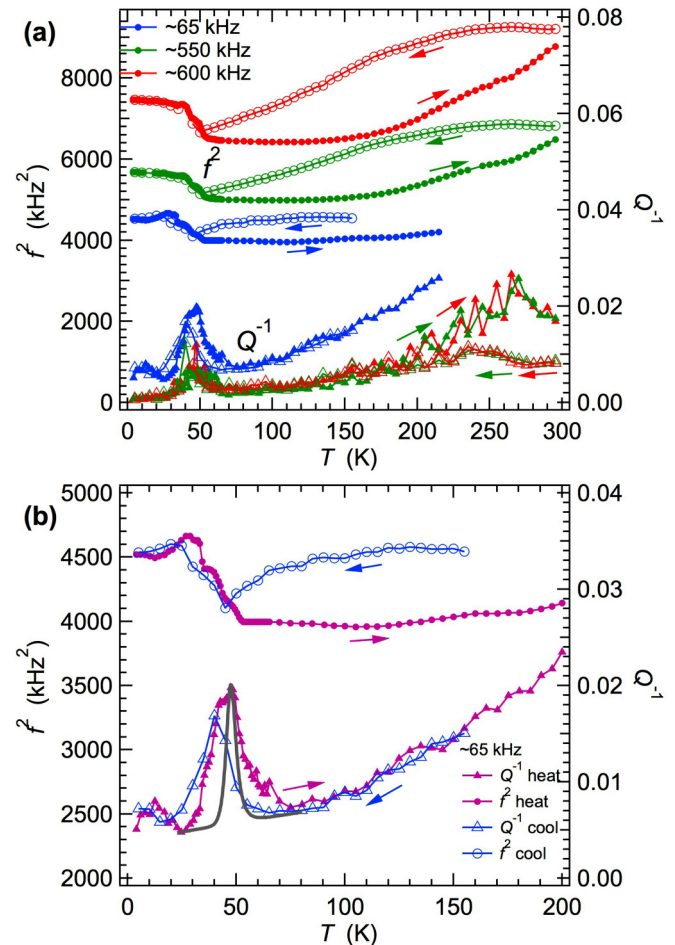

FIG. 7. (a) Variations of f^2 (circles) and Q^{-1} (triangles) from three different resonances during cooling (open symbols) and heating (filled symbols); f^2 values have been rescaled so that data for all three resonances can be compared on the same diagram. (b) Details of the resonance with frequency near 65 kHz. Arrows indicate the direction of changing temperature in the cooling and heating sequences.

in the ab plane. From the analysis reported here, there is a high likelihood that at least one phase transition occurs in the region of 25–50 K. Variable temperature PXRD was used in an attempt to probe any possible changes in structures. This suggests no systematic change in cell parameters or refinement parameters exist for KLT. However, this does not exclude the possibility that a phase transition occurs in this range. Subtle octahedral tilts rely on exact refinement of O positions. Those reported [63] in $Ba_4(La_{1-x}Nd_x)_{0.67}Nb_{10}O_{30}$ are not likely to be seen in PXRD analysis, especially in KLT, due to the presence of heavier Ta. In addition, these subtle tilts affect the ferroelectric properties, as shown [64] in $(Sr_xBa_{1-x})_5Nb_{10}O_{30}$. Neutron diffraction studies are required to probe O and Li effects on structure further.

It is important to try to reconcile the specific heat data and the dielectric data. Specific heat is a quasistatic, not dynamic, measurement for probing any phase transition. This is equivalent to probing the sample in the zero-frequency (dc) limit; therefore the phase transition, in theory, would occur at the freezing temperature T_f extrapolated from dielectric

data. However, a feature for T_{f1} in ε' is not visible in the measurement window since the linear temperature dependence follows a polynomial trend line. When the specific heat is plotted against T^3, no features are seen. However, the Debye temperature, where classical fluctuations dominate and data should plateau, is well above the freezing temperatures from our Vogel-Fulcher fits. This suggests that quantum fluctuations are involved in the dielectric transitions seen.

The transitions reported here are at higher temperatures than those reported in the literature. For the single crystal data [34], T_c is reported as 7 K at an unknown frequency, with samples being stoichiometric for both KLT and KLN. This claim for KLN is in direct contradiction to later papers where Fukuda reports [34,65] that KLT and KLN have C sites completely filled with Li and both A1 and A2 with K, but later papers which say an excess of Nb is required for KLN to form [24–28]. Therefore, there is a slim chance that the lower reported transition temperature could be due to contamination, as widely known for $BaTiO_3$, or deviation from stoichiometric KLT in samples. However, without further information, resolving this difference is not possible. For ceramic samples [24], similar data down to 100 K are seen, especially in samples that have $P4/mbm$ symmetry at lower partial pressures of K and Li. New to this work are the two frequency dependent peaks, which imply relaxor dielectric properties for KLT, which is very similar to KLN. The ferroelectric transition in KLN is already known to be frequency dependent, with a dielectric permittivity maximum shifting around 750 K [40]. These two relaxor-type peaks from KLT may be explained in terms of partial occupancies or mixing of the sites in the TTB, since both explanations have been reported in KLN [28,66], alternatively incommensurate transitions may occur, as reported [21] with other TTB compounds. Which of these exist in KLT will be the subject of further (neutron scattering) investigations

The Vogel-Fulcher relationship gives the best fit to our experimental dielectric data. Vogel-Fulcher fits suggest that two different relaxation mechanisms occur with KLT, with the activation energies and attempt frequencies being of a similar magnitude for each mechanism. The large variation in the freezing temperatures between ε' and ε'' is a reflection of the T_m values for ε' occur at a higher temperature than T_m values for ε'' shifting the whole Vogel-Fulcher fit to higher temperatures in ε' without strongly altering the shape. It is not generally necessary that ε' and ε'' peaks are at the same temperature. The freezing temperatures are of interest as a prediction of where the structural transition would occur, if it exists. T_{f2} is negative, extrapolated as either -5.0 or -15.0 K (from ε' or ε''); therefore a static structural transition is unlikely to occur at a finite temperature, implying a glassy $T = 0$ ground state. Negative freezing temperature has been seen previously in hexaferrites [11] and explained by a degenerate glassy ground state occurring at absolute zero generated by the existence of quantum fluctuations. Probing this sample with very low frequency (sub-Hz) for example with a torsional pendulum would, in theory, shift the transition to absolute zero, suggesting that there is at least one relaxor-type QCP in KLT.

With the immittance spectroscopy data, the responses are interpreted as coming from within the grains, with a small electrode spike at low frequency and higher temperatures; no evidence of grain boundary relaxation is observed. The

Arrhenius plot generates two activation energies, which is similar to KLN data reported by Jun *et al.* [67]. The lower temperature range, approximately 600–700 K, has reported [67] activation energies of 0.90 and 0.83 eV for KLT and KLN, respectively. However, the activation energies for KLN and KLT reported [67,68] vary depending on the sample, both in terms of temperature range for linear Arrhenius plots and obtained values for activation energies. As suggested for KLN, the two mechanisms seen in KLT are likely to be linked by Li ion motion, although the activation energies reported here are less than 1.27 eV reported for Li ionic conduction in $LiTaO_3$ [69] but comparable for other TTBs [70] containing Li, with activation energies of around 0.80 eV. At > 0.6 eV the activation energies for KLT are larger than the reported values of 0.15 and 0.12 eV for LiO_2 and Li_2CO_3 [71,72]. However, for commercial applications, the ionic current per unit weight is a key parameter, and tantalate or niobate tungsten bronzes are not competitive with lighter weight Li oxides, carbonates, or sulfides.

If there is a phase transition in KLT at low temperatures, it does not conform to the normal expectations of strain coupling. A ferroelastic transition with linear/quadratic strain/order ($\lambda e Q^2$) would be expected to give significant elastic softening below the transition point [73,74], but this is not observed. Bilinear coupling of the driving order parameter with the symmetry breaking shear strain for a discrete phase transition ($\lambda e Q$) would give rise to the standard pattern of softening to a minimum at the transition point followed by recovery below it, but, as discussed above, the only direct evidence for a ferroelastic transition is that it would occur above room temperature. The initial trend of elastic softening with falling temperature seen in Fig. 7 is more likely to have a dynamic origin and the best analogy may be with the softening seen in RUS data from $Pb(Mg_{1/3}Nb_{2/3})O_3$ (PMN) [75]. In PMN the softening is attributed to the development of dynamical polar nanoregions (PNRs) at temperatures between the Burns temperature of $\sim$630 K and the temperature interval within which they freeze, 230–270 K. The relaxor freezing process is then accompanied by elastic stiffening and a peak in the acoustic loss. However, the latter extends down to at least $\sim$10 K, rather than occurring more discretely in the much narrower temperature interval of $\sim$40 K seen here for KLT.

The pattern for elastic and anelastic effects in KLT thus appears to be of softening due to dynamical effects, such as the condensation of PNRs, followed by discrete pinning or freezing of defects which couple with strain. Changes in dielectric constant and dielectric loss in PMN have the same general form as changes in elastic compliance and acoustic loss, but with significant differences in detail. This was attributed to the fact that the ac electric field produces responses primarily from 180° twin walls, which are not coupled with shear strain, whereas an ac stress produces responses only from 90° twin walls [75]. In KLT there are two dielectric anomalies, centered at 46 and 69 K when measured at 316 kHz, and one elastic anomaly, centered at $\sim$47 K measured at $\sim$65 kHz. The simplest explanation of the discrepancy is that the higher temperature anomaly involves only 180° switching of local ferroelectric moments while the lower temperature anomaly involves 90° switching, as if the two types of boundaries

between PNRs or two types of ferroelectric domain walls freeze at different temperatures. Activation energies extracted from the RUS data are sufficiently close to those extracted from the dielectric data to suggest that the same pinning or freezing process is being sampled.

There are also significant differences between RUS results from KLT and PMN, such as the hysteresis seen for KLT. It is possible that the differences in f^2 and Q^{-1} between cooling and heating in the temperature range $\sim 50-295$ K are due to opening up of grain boundaries associated with changes in volume due to structural changes below ~ 50 K. This effect has been seen, for example, when a polycrystalline sample of quartz with grain sizes in the range 0.1–0.3 mm is heated through the α-β transition [76], except that opening of the grain boundaries causes the polycrystalline sample to become elastically softer rather than stiffer, as here. The broad peaks at ~ 270 K in the heating sequence and at ~ 240 K in the cooling sequence [Fig. 7(a)] are reminiscent of broad peaks seen at ~ 200 K in RUS data collected from $Ba_2NaNb_5O_{15}$ (BNN) [77] and an alternative explanation is that the loss is associated with pinning (during cooling) and unpinning (during heating) of ferroelastic twin walls in both materials. This would be analogous to the anelastic behavior of twin walls in improper ferroelastic perovskites [78]. The sequences of structural changes in BNN and KLT are not the same but a feature in common is that both could undergo tetragonal-orthorhombic transitions during cooling such that both would contain ferroelastic twin walls. At room temperature the twin walls form a classic tweed pattern in BNN [79,80] while they appear for $x \gtrsim 0.7$ but are visibly more sparse in $K_3Li_2Ta_5O_{15}$ [34]. There appear to have been no previous optical studies of KLT, but examination of crushed grains mounted in oil using a polarized light microscope has provided some indication that the expected ferroelastic twinning was present in the sample of KLT used for the present study. Changes in the proportions of differently oriented ferroelastic twin domains in a single crystal would also cause changes in the effective elastic constants of the crystal as a whole. Hysteretic effects would then arise in KLT if reorientation of twin walls occurs within individual grains of a ceramic sample, rather than opening up of grain boundaries, in response to stresses at grain boundaries which develop as a consequence of the structural changes at ~ 50 K and below.

To conclude, the tetragonal tungsten bronze-type structure of KLT has a room temperature structure that depends on the synthesis conditions. With lower partial pressures of K and Li giving lower K content, a tetragonal $P4/mbm$ structure is observed. At higher pressures of K and Li in synthesis, near stoichiometric values for K:Ta orthorhombic $Cmmm$ structure are obtained. Characterization of the higher partial pressures near stoichiometric pellets showed that features observed depend on both method of analysis and frequency used. Two dielectric peaks are seen in the range 316 Hz to 1 MHz which fit Vogel-Fulcher analysis, with extrapolation giving transition temperatures above and below absolute zero. The transition above 0 K may be linked to the feature in RUS data and a change in structure. However, further work is required to reconcile these differences. The transition that is extrapolated to below 0 K is explained by a degenerate glassy ground state at 0 K created by quantum fluctuations, implying a relaxor-type

ferroelectric QCP occurs in KLT. Thus studies of quantum critical points should be extended to such tungsten bronzes.

III. PYROCHLORE LEAD NIOBATE

A. Pyrochlore structure

Similar results to KLT, of peaks with the dielectric permittivity but not in heat capacity, are seen with pyrochlores $Pb_2Nb_2O_7$ and $Cd_2Nb_2O_7$. The structure of $Cd_2Nb_2O_7$ is a cubic $Fd-3m$ pyrochlore, however, due to the increase size and/or lone pair on Pb. A stacking fault occurs every nine layers, creating a trigonal $P3m1$ pyrochlore structure [81]. For $Pb_2Nb_2O_7$ a long-term controversy has existed with Hulm [82] and, independently, Pepinsky and Shirane [83] discovering in lead pyrochlore a ferroic [probably not ferroelectric since it exhibits "quite" linear unsaturated $P(E)$ hysteresis loop] transition at $T \approx +15.4$ K, but Siegwarth *et al.* [84] argued vehemently that there is no such phase transition, and that these are electret effects. It is now generally established that cadmium niobium pyrochlore is glassy below 18 or 19 K, but the lead pyrochlore is more enigmatic and controversial. We reconcile these claims by reanalyzing the literature to show that this material is also a relaxor QCP, with a dielectric peak at $T \approx 15.4$ K at kHz probe frequencies f, but no anomalies for $T > 0$ K in specific heat or XRD measurements. Hence, this pyrochlore is another relaxor QCP that can be frequency tuned to exhibit dielectric permittivity maximum at $T = 0$ K.

B. Pyrochlore reanalysis literature section

This controversy regarding pyrochlore $Pb_2Nb_2O_7$, with Hulm, Pepinsky, and others reporting [82,83,85,86] a phase transition (ferroelectric) at $T = 14.0-15.4$ K but Siegwarth *et al.* [84] and Lawless [87] argued strongly that this was some sort of defect relaxation continues 50 years as moot until the present day.

Our interpretation of the literature is different from that of Siegwarth *et al.* [84], shown in Fig. 8: This is not relaxation of defects, but a relaxor ferroelectric transition. Our Vogel-Fulcher fit to their original data is displayed in Fig. 9, showing the obtained solutions when a free fit and constraint fit for f_0 are undertaken. When unconstrained fit is used, the value for f_0 is unrealistic; there are simply too few data points to fit f_0, and the values of f_0 and E_a obtained are highly correlated. Note that this very low-temperature transition is different from the relaxor transition [88] in $Cd_2Nb_2O_7$ at $T_c = 196$ K.

Ubic and Reaney [81] show that oxygen vacancies in typical lead pyrochlores result in a lowering of symmetry to trigonal. Thus data can be sample dependent. This also suggests that lead-niobate pyrochlore may be trigonal below 15.4 K. Jayaraman *et al.* [89] showed, in a rarely cited study on an excellent single crystal of stoichiometric $Pb_2Nb_2O_7$ pyrochlore, that the ferroelectric phase transition could be reached at a hydrostatic pressure of 4.5 GPa and that after the release of such applied pressure the structure reverted to rhombohedral (trigonal). We speculate that the phase above 4.5 GPa at 292 K is the same ferroelectric phase as that below $T = 15.4$ K at ambient pressure. Shrout and Swartz [90] show that lead magnesium niobate also has a relaxor-like transition at a similar cryogenic temperature ($T = 20$ K). The phase
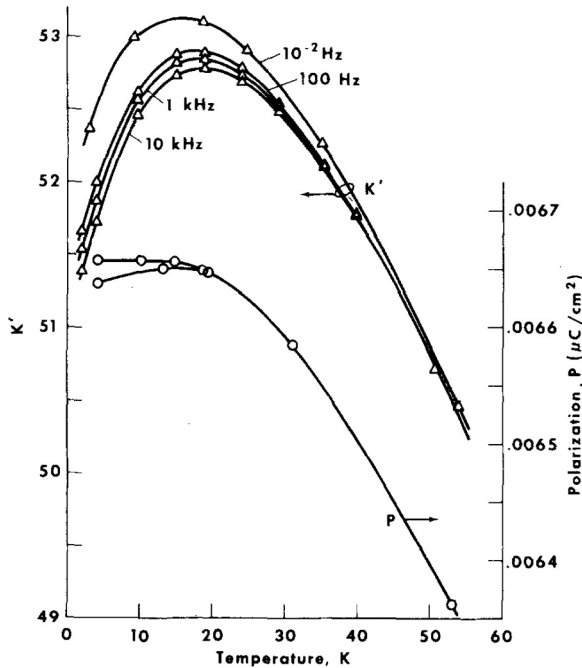
FIG. 8. Reprinted from J. D. Siegwarth *et al.*, J. Appl. Phys. **47**, 3789 (1976), with the permission of AIP Publishing. Note the extremely small polarization of nC/cm^2 [88] gives $2.1\,\mu C/cm^2$ for $Cd_2Nb_2O_7$ in this temperature range [monoclinic space group $P2_1$ ($1a$ in Fedorov notation) below $T(\text{lock}-\text{in}) = 46$ K]—nearly $1000\times$ greater.

diagram in $Cd_2Nb_2O_7$ is already known to be complicated [91–100], with seven phases, including an incommensurate one that locks in to monoclinic below $T(\text{lock}-\text{in}) = 46$ K, and a glassy phase below $T_g = 19$ K. $Pb_2Nb_2O_7$ has been more controversial. It is already known that mixed pyrochlores of formula $(Cd, Pb)_2(Nb, Ta)_2O_7$ can be quantum ferroelectrics with Curie temperatures T_c passing through zero [101] We note that the lanthanide pyrochlores also have phase transitions in the temperature range near $T = 20$ K [102,103]. These have been interpreted as magnetically driven, but we suspect that they are typical of most pyrochlores and independent of magnetism.

Siegwarth and Lawless [84] report a very small pyrochlore polarization of $6\,nC\,cm^{-2}$ for Pb-niobate. They published details of the equipment, in 1971, with such sensitive capabilities [104]. However, although their equipment was very good, their samples were not. In a new 2017 book [105], it is pointed out that Siegwarth and Lawless never achieved a densification greater than 75% for their lead pyrochlore samples. Perhaps even more important, Sekiya *et al.* [106] found, unlike most authors, that $Pb_2Nb_2O_7$ is ferroelectric. They concluded that rapid quenching is important (metastable phases) and that the samples also require a high-temperature anneal after growth, following which the dielectric constant rapidly increases. In addition, the annealing temperature will affect whether mixed phases or a single phase formed [107]. So the conclusion is that ferroelectricity in lead pyrochlore may depend upon stoichiometry, densification, and annealing procedure.

We have prepared our own samples of lead pyrochlore. However, these differ from those studied previously either by
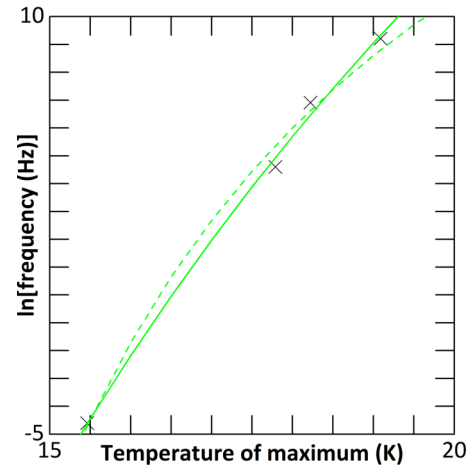
Free fit : $T_f = -1.4$ K; $E_a = 0.12$ eV;

$f_0 = 1.85 \times 10^{+32}$ Hz;

SSR $= 0.3238 \ln(Hz)^2$,

Constrained f_0 fit : $T_f = +9.8$ K; $E_a = 0.017$ eV;

$f_0 = 1 \times 10^{+13}$ Hz;

SSR $= 0.8418 \ln(Hz)^2$.

FIG. 9. Our Vogel-Fulcher fits to the original data of Siegwarth *et al.* [84], first using a free fit model (solid line) generating an attempt frequency f_0 that is unrealistic, hence a constrained model with $f_0 = 1 \times 10^{13}$ also shown (dashed lines). The lack of data points causes the parameters f_0 and E_a in the fit to be highly correlated and not independent.

improved stoichiometry that requires additional data and will be reported separately. But the main point is that we find that the dielectric permittivity monotonically increases as temperature is lowered from $T = 300$ to 14 K, at which point it plateaus. This is compatible with a real phase transition near $10-15$ K.

To conclude, the reanalysis of literature, with a free fit VF model, suggests that this is a relaxor-type ferroelectric with low-temperature transition which for dc measurements is below absolute zero. This explanation will require experimental confirmation that may be the subject of a future paper.

IV. CONCLUSIONS

In summary, we present evidence for two new relaxor-type QCP in tetragonal tungsten bronze, $K_3Li_2Ta_5O_{15}$, and in lead pyrochlore, $Pb_2Nb_2O_7$, using literature as well as new experimental data for KLT. KLT is revealed to be a glassy relaxor with freezing temperatures at or below absolute zero, whose dielectric permittivity peaks occur at temperatures that can, therefore, be fine tuned through absolute zero via frequency. The relaxor theory of Tagantsev is confirmed. Thus they may be of interest as glassy QCP systems, adding to the list of QCP candidates that already includes perovskites and hexaferrites. Note, however, that some subtlety is involved in discriminating between relaxor ferroelectrics and dipole glasses via Vogel-Fulcher equations [108,109]. However, further investigations, especially structural, are required for both since, as with

other cryogenic ferroelectric such as $CdTiO_3$ [110,111] the controversy will continue.

ACKNOWLEDGMENTS

[1] S. E. Rowley, L. J. Spalek, R. P. Smith, M. P. M. Dean, M. Itoh, J. F. Scott, G. G. Lonzarich, and S. S. Saxena, Nat. Phys. **10**, 367 (2014).

[2] J. F. Scott, A. Schilling, S. E. Rowley, and J. M. Gregg, Sci. Technol. Adv. Mater. **16**, 036001 (2015).

[3] S. E. Rowley, Y.-S. Chai, S.-P. Shen, Y. Sun, A. T. Jones, B. E. Watts, and J. F. Scott, Sci. Rep. **6**, 25724 (2016).

[4] S.-P. Shen, J.-C. Wu, J.-D. Song, X.-F. Sun, Y.-F. Yang, Y.-S. Chai, D.-S. Shang, S.-G. Wang, J. F. Scott, and Y. Sun, Nat. Commun. **7**, 10569 (2016).

[5] P. Chandra, G. G. Lonzarich, S. E. Rowley, and J. F. Scott, Rep. Prog. Phys. **80**, 112502 (2017).

[6] H. B. Cao, Z. Y. Zhao, M. Lee, E. S. Choi, M. A. Mcguire, B. C. Sales, H. D. Zhou, J.-Q. Yan, and D. G. Mandrus, APL Mater. **3**, 062512 (2015).

[7] S. E. Rowley, M. Hadjimichael, M. N. Ali, Y. C. Durmaz, J. C. Lashley, R. J. Cava, and J. F. Scott, J. Phys. Condens. Matter **27**, 395901 (2015).

[8] J. C. Lashley, J. H. D. Munns, M. Echizen, M. N. Ali, S. E. Rowley, and J. F. Scott, Adv. Mater. **26**, 3860 (2014).

[9] F. Kagawa, N. Minami, S. Horiuchi, and Y. Tokura, Nat. Commun. **7**, 10675 (2016).

[10] F. Kagawa, S. Horiuchi, and Y. Tokura, Crystals **7**, 106 (2017).

[11] S. E. Rowley, T. Vojta, A. T. Jones, W. Guo, J. Oliveira, F. D. Morrison, N. Lindfield, E. Baggio Saitovitch, B. E. Watts, and J. F. Scott, Phys. Rev. B **96**, 020407(R) (2017).

[12] J. F. Scott, Crystals **8**, 180 (2018).

[13] A. Rotaru, D. C. Arnold, A. Daoud-Aladine, and F. D. Morrison, Phys. Rev. B **83**, 184302 (2011).

[14] A. Rotaru and F. D. Morrison, J. Therm. Anal. Calorim. **120**, 1249 (2015).

[15] D. Viehland, S. J. Jang, L. E. Cross, and M. Wuttig, J. Appl. Phys. **68**, 2916 (1990).

[16] R. Pirc and R. Blinc, Phys. Rev. B **76**, 020101(R) (2007).

[17] B. E. Vugmeister, Phys. Rev. B **73**, 174117 (2006).

[18] M. Trainer, American Journal of Physics **69**, 966 (2001).

[19] R. J. D. Tilley, Int. J. Refract. Met. Hard Mater. **13**, 93 (1995).

[20] A. Simon and J. Ravez, Comptes Rendus Chim. **9**, 1268 (2006).

[21] X. Zhu, M. Fu, M. C. Stennett, P. M. Vilarinho, I. Levin, C. A. Randall, J. Gardner, F. D. Morrison, and I. M. Reaney, Chem. Mater. **27**, 3250 (2015).

[22] R. Guo, A. S. Bhalla, C. A. Randall, Z. P. Chang, and L. E. Cross, J. Appl. Phys. **67**, 1453 (1990).

[23] J. F. Scott, A. Shawabkeh, W. F. Oliver, A. C. Larson, and P. J. Vergamini, Ferroelectrics **104**, 85 (1990).

[24] M.-S. Kim, J.-H. Lee, J.-J. Kim, H. Y. Lee, and S.-H. Cho, Integr. Ferroelectr. **69**, 11 (2005).

[25] G. Y. Kang and J. K. Yoon, J. Cryst. Growth **193**, 615 (1998).

[26] C.-Y. Jang, J.-H. Lee, J.-J. Kim, S.-H. Cho, and H. Y. Lee, J. Electroceram. **13**, 847 (2004).

[27] A. Peter, I. Hajdara, K. Lengyel, G. Dravecz, L. Kovacs, and A. Toth, J. Alloys Compd. **463**, 398 (2008).

[28] S. C. Abrahams, P. B. Jamieson, and J. L. Bernstein, J. Chem. Phys. **54**, 2355 (1971).

[29] C. Li, J. Han, J. Wang, L. Zhang, and H. Zhao, Chinese Phys. Lett. **14**, 468 (1997).

[30] Y. Xu, Z. Li, W. Li, H. Wang, and H. Chen, Phys. Rev. B **40**, 11902 (1989).

[31] Z. Lu, J.-P. Bonnet, J. Ravez, and P. Hagenmuller, J. Mater. Sci. **30**, 5819 (1995).

[32] W. Zhong, P. Zhang, H. Zhao, Z. Han, and H. Chen, Chinese Phys. Lett. **10**, 183 (1993).

[33] R. D. Shannon, Acta Crystallogr. **A32**, 751 (1976).

[34] T. Fukuda, Jpn. J. Appl. Phys. **9**, 599 (1970).

[35] M. Takashige, S.-I. Hamazaki, M. Tsukioka, F. Shimizu, H. Suzuki, and S. Sawada, J. Phys. Soc. Jpn. **62**, 1486 (1993).

[36] M. Takashige, S. Kojima, S.-I. Hamazaki, F. Shimizu, and M. Tsukioka, Jpn. J. Appl. Phys. **32**, 4384 (1993).

[37] M. Tsukioka, S. Hamazaki, M. Takashige, F. Shimizu, H. Suzuki, and S. Sawada, J. Phys. Soc. Jpn. **61**, 4669 (1992).

[38] S. Kojima, S. Hamazaki, M. Tsukioka, and M. Takashige, J. Phys. Soc. Jpn. **62**, 1097 (1993).

[39] S. Mori, N. Yamamoto, Y. Koyama, S. Hamazaki, and M. Takashige, Phys. Rev. B **52**, 9117 (1995).

[40] H. Ivett, Ph.D. thesis, University of Pécs, 2013.

[41] H. M. Rietveld, J. Appl. Crystallogr. **2**, 65 (1969).

[42] B. H. Toby, J. Appl. Crystallogr. **34**, 210 (2001).

[43] A. C. Larson and R. B. Von Dreele, General Structure Analysis System (GSAS), Los Alamos National Laboratory Report LAUR 86-748 (1994).

[44] A. Migliori and J. L. Sarrao, in *Resonant Ultrasound Spectroscopy: Applications to Physics, Material Measurements and Nondestructive Evaluation* (Wiley, New York, 1997), p. 201.

[45] J. Schiemer, L. J. Spalek, S. S. Saxena, C. Panagopoulos, T. Katsufuji, A. Bussmann-Holder, J. Köhler, and M. A. Carpenter, Phys. Rev. B **93**, 054108 (2016).

[46] D. M. Evans, J. A. Schiemer, M. Schmidt, H. Wilhelm, and M. A. Carpenter, Phys. Rev. B **95**, 094426 (2017).

[47] G. E. P. Box, Biometrika **40**, 318 (1953).

[48] A. K. Tagantsev, Phys. Rev. Lett. **72**, 1100 (1994).

[49] E. Nakamura, T. Mitsui, and J. Furuichi, J. Phys. Soc. Jpn. **18**, 1477 (1963).

[50] R. Flores-Ramirez, A. Huanosta, E. Amano, R. Valenzuela, and A. R. West, Ferroelectrics **99**, 195 (1989).

[51] M. A. Carpenter, E. K. H. Salje, and C. J. Howard, Phys. Rev. B **85**, 224430 (2012).

[52] M. A. Carpenter and Z. Zhang, Geophys. J. Int. **186**, 279 (2011).

[53] M. A. Carpenter, C. J. Howard, R. E. A. McKnight, A. Migliori, J. B. Betts, and V. R. Fanelli, Phys. Rev. B **82**, 134123 (2010).

[54] M. Weller, G. Y. Li, J. X. Zhang, T. S. Kê, and J. Diehl, Acta Metall. **29**, 1047 (1981).

[55] A. S. Nowick and B. S. Berry, *Anelastic Relaxation in Crystalline Solids* (Academic, New York, 1972).

[56] W. F. Oliver and J. F. Scott, Ferroelectrics **117**, 63 (1991).

[57] P. W. Young and J. F. Scott, Phase Trans. **6**, 175 (1986).

[58] J. F. Scott, S.-J. Sheih, and T. Chen, Ferroelectrics **117**, 21 (1991).

[59] J. F. Scott and S.-J. Sheih, J. Phys. Condens. Matter **2**, 8553 (1990).

[60] J. F. Scott, S. A. Hayward, and M. Miyake, J. Phys. Condens. Matter **17**, 5911 (2005).

[61] C. Filipic, Z. Kutnjak, R. Lortz, A. Torres-Pardo, M. Dawber, and J. F. Scott, J. Phys. Condens. Matter **19**, 236206 (2007).

[62] J. Gardner and F. D. Morrison, Dalton Trans. **43**, 11687 (2014).

[63] J. Gardner, F. Yu, C. Tang, W. Kockelmann, W. Zhou, and F. D. Morrison, Chem. Mater. **28**, 4616 (2016).

[64] G. H. Olsen, U. Aschauer, N. A. Spaldin, S. M. Selbach, and T. Grande, Phys. Rev. B **93**, 180101(R) (2016).

[65] T. Fukuda, Jpn. J. Appl. Phys. **8**, 122 (1969).

[66] S.-L. Xu, J.-H. Lee, J.-J. Kim, H. Y. Lee, and S.-H. Cho, Mater. Sci. Eng. **B99**, 483 (2003).

[67] B. E. Jun, S. C. Song, D. J. Kim, C. S. Kim, G. S. Jeen, H. K. Kim, J. N. Kim, and Y. Hwang, J. Korean Phys. Soc. **42**, S1252 (2003).

[68] J. S. Kim, D. J. Kim, and J. N. Kim, J. Korean Phys. Soc. **32**, S316 (1998).

[69] D. C. Sinclair and A. R. West, Phys. Rev. B **39**, 13486 (1989).

[70] V. Hornebecq, J. M. Reau, and J. Ravez, Solid State Ionics **127**, 231 (2000).

[71] L. Benitez and J. M. Seminario, J. Electrochem. Soc. **164**, E3159 (2017).

[72] Y. C. Chen, C. Y. Ouyang, L. J. Song, and Z. L. Sun, J. Phys. Chem. C **115**, 7044 (2011).

[73] M. A. Carpenter and E. K. H. Salje, Eur. J. Mineral. **10**, 693 (1998).

[74] W. Rehwald, Adv. Phys. **22**, 721 (1973).

[75] M. A. Carpenter, J. F. J. Bryson, G. Catalan, S. J. Zhang, and N. J. Donnelly, J. Phys. Condens. Matter **24**, 045902 (2012).

[76] R. E. A. McKnight, T. Moxon, A. Buckley, P. A. Taylor, T. W. Darling, and M. A. Carpenter, J. Phys. Condens. Matter **20**, 075229 (2008).

[77] J. Herrero-Albillos, P. Marchment, E. K. H. Salje, M. A. Carpenter, and J. F. Scott, Phys. Rev. B **80**, 214112 (2009).

[78] M. A. Carpenter, J. Phys. Condens. Matter **27**, 263201 (2015).

[79] L. G. Van Uitert, J. J. Rubin, and W. A. Bonner, IEEE J. Quantum Electron. **4**, 622 (1968).

[80] J. S. Abell, K. G. Barraclough, I. R. Harris, A. W. Vere, and B. Cockayne, J. Mater. Sci. **6**, 1084 (1971).

[81] R. Ubic and I. M. Reaney, J. Am. Ceram. Soc. **85**, 2472 (2002).

[82] J. K. Hulm, Phys. Rev. **92**, 504 (1953).

[83] G. Shirane and R. Pepinsky, Phys. Rev. **92**, 504 (1953).

[84] J. D. Siegwarth, W. N. Lawless, and A. J. Morrow, J. Appl. Phys. **47**, 3789 (1976).

[85] F. Jona, G. Shirane, and R. Pepinsky, Phys. Rev. **98**, 903 (1955).

[86] I. S. Zheludev, in *Physics of Crystalline Dielectrics* (Springer, Heidelberg, 2012), p. 78.

[87] W. N. Lawless, Phys. Rev. B **19**, 3755 (1979).

[88] N. N. Kolpakova, P. Charnetzki, W. Nawrochik, P. P. Syrnikov, and A. O. Lebedev, J. Exp. Theor. Phys. **94**, 395 (2002).

[89] A. Jayaraman, G. A. Kourouklis, A. S. Cooper, and G. P. Espinosa, J. Phys. Chem. **94**, 1091 (1990).

[90] T. R. R. Shrout and S. L. L. Swartz, Mater. Res. Bull. **18**, 663 (1983).

[91] W. N. Lawless, A. C. Anderson, and F. Walker, Ferroelectrics **37**, 627 (1981).

[92] N. N. Kolpakova, B. Hilczer, and M. Wiesner, Phase Trans. **47**, 113 (1994).

[93] N. N. Kolpakova and P. Czarnecki, J. Exp. Theor. Phys. **100**, 964 (2005).

[94] N. N. Kolpakova, J. Exp. Theor. Phys. **96**, 538 (2003).

[95] N. N. Kolpakova, P. Czarnecki, W. Nawrocik, M. P. Shcheglov, P. P. Syrnikov, and L. Szczepańska, Phys. Rev. B **72**, 024101 (2005).

[96] E. Buixaderas, S. Kamba, J. Petzelt, M. Savinov, and N. N. Kolpakova, Eur. Phys. J. B **19**, 9 (2001).

[97] Z. G. Ye, N. N. Kolpakova, J.-P. Rivera, and H. Schmid, Ferroelectrics **124**, 275 (1991).

[98] N. N. Kolpakova, M. Wiesner, G. Kugel, and P. Bourson, Ferroelectrics **190**, 179 (1997).

[99] N. N. Kolpakova, P. Czarnecki, W. Nawrocik, M. P. Shcheglov, and A. O. Lebedev, Ferroelectrics **291**, 125 (2003).

[100] N. N. Kolpakova, R. Margraf, and M. Polomska, J. Phys. Condens. Matter **6**, 2787 (1994).

[101] C. F. Clark, W. N. Lawless, and A. S. Bhalla, Jpn. J. Appl. Phys. **24**, 266 (1985).

[102] X. W. Dong, K. F. Wang, S. J. Luo, J. G. Wan, and J.-M. Liu, J. Appl. Phys. **106**, 104101 (2009).

[103] T. Katsufuji and H. Takagi, Phys. Rev. B **69**, 064422 (2004).

[104] W. N. Lawless, Rev. Sci. Instrum. **42**, 561 (1971).

[105] M. T. Sebastian, R. Ubic, and H. Jantunen, in *Microwave Materials and Applications* (Wiley, Hoboken, NJ, 2017), p. 181.

[106] T. Sekiya, A. Tsuzuki, S. Kawakami, and Y. Torii, Mater. Res. Bull. **24**, 63 (1989).

[107] K. Sreedhar and A. Mitra, J. Am. Ceram. Soc. **82**, 1070 (1999).

[108] Z. Kutnjak and R. Pirc, J. Appl. Phys. **121**, 105107 (2017).

[109] R. Pirc and Z. Kutnjak, Phase Trans. **88**, 222 (2015).

[110] A. I. Lebedev, Phys. Solid State **51**, 802 (2009).

[111] B. J. Kennedy, Q. Zhou, and M. Avdeev, J. Solid State Chem. **184**, 2987 (2011).